Thin-film transformations and volatile products in the formation of nanoporous low-*k* polymethylsilsesquioxane-based dielectric

P. Lazzeri, L. Vanzetti, M. Anderle, and M. Bersani
ITC-irst, via Sommarive 18, 38050 Povo, Trento, Italy

J. J. Park,[a] Z. Lin, R. M. Briber, and G. W. Rubloff[a),b)]
Department of Materials Science and Engineering, University of Maryland, College Park, Maryland 20742-3285

H. C. Kim and R. D. Miller
IBM Almaden Research Center, 650 Harry Road, San Jose, California 95120-6099

(Received 22 September 2004; accepted 7 March 2005; published 19 May 2005)

The thermal transformation of spin-cast thin films to produce nanoporous low-*k* dielectric layers has been investigated using polymethysilsesquioxane (PMSSQ) for the low-*k* matrix and polymethylmethacrylate-co-dimethylaminoethylacrylate (PMMA-co-DMAEMA) as the porogen which is volatilized to leave nanopores in the matrix. Surface analysis methods, including time of flight-secondary ion mass spectrometry and x-ray photoelectron spectroscopy, and thin film analysis by small-angle neutron scattering revealed the kinetics of matrix crosslinking, while thermal desorption mass spectrometry showed the evolution of gaseous reaction products from porogen and matrix during the complex chemical transformations which occur with thermal cycling from 100 °C to 450 °C. Matrix crosslinking occurs primarily at lower temperatures (100–225 °C), while porogen diffusion and decomposition begins somewhat above 200 °C, leading to phase separation which creates the final nanoporous structure. Since matrix and porogen reaction kinetics have some overlap, relative kinetics can be important: e.g., matrix crosslinking proceeds more rapidly for PMSSQ precursors with high Si–OH content cf. low SiOH content, with implications for the morphology of porogen-derived nanostructure. As surface species transform (matrix crosslinking) and disappear (porogen volatilization), their complements are seen in the gas phase as reaction and decomposition products. Porogen decomposition is ligand selective, in that the N-containing ligand of DMAEMA is volatilized at considerably lower temperatures (~200 °C) than that (~400 °C) for the remaining species (the PMMA ligand and the common backbone for both PMMA and DMAEMA). © *2005 American Vacuum Society.* [DOI: 10.1116/1.1900734]

I. INTRODUCTION

With shrinking microelectronic device feature sizes and complex wiring networks in Si technology, signal transport across wiring structures has become a significant limitation to circuit-level speed. This has forced a fundamental paradigm shift for interconnect technology, in particular to lower resistivity metals (Cu based) and to lower dielectric constant insulators (low *k*), along with associated process and integration strategies.[1]

Recently, there have been many efforts to develop low-*k* materials, and many candidates have been introduced, such as organic materials, silica-based materials, and organosilicates.[2,3] Inorganic-based materials, such as C-doped silica[4] and organosilicates,[2] have been recognized as candidates to meet the thermal and mechanical requirements since they take advantage of the physical properties of the rigid Si–O bonding network. Even though there are still thermal decomposition problems for some of the materials at an elevated temperature,[5] these materials usually show better thermal and mechanical performance than purely organic materials at the processing temperatures near 450 °C which are required for interconnect technology.[3]

The demands of the technology on material performance and process compatibility are stringent, so that at this point it is still not clear whether plasma-enhanced chemical vapor deposition or spin-cast low-*k* dielectrics will become the strategy of choice. Some would argue that thermal processing of spin-cast materials is an approach more extendible to highly porous low-*k* structures, so that lower effective *k* values can be obtained. For spin-cast materials based on $Si-O-CH_3$ networks, silsesquioxane ($RSiO_{1.5}$), organosilicate-based material with various terminal groups are particularly attractive. Low-*k* values are achieved by incorporating nonpolar, space-occupying large atoms or molecules, such as H or CH_3, to achieve low polarizability and lower the density of this material.[6–8]

While these materials offer dielectric constants in the range of $2<k<3$, ultra low-*k* materials ($k<2.0$) are required for sub-65 nm technology. Lower *k* values achievable in continuous materials are not accompanied by the thermal stability required for next-generation interconnect technology. Instead, much attention is now focused on the develop-

[a)]Also at: Institute for Systems Research, University of Maryland, College Park, MD 20742-3285.
[b)]Electronic mail: rubloff@isr.umd.edu

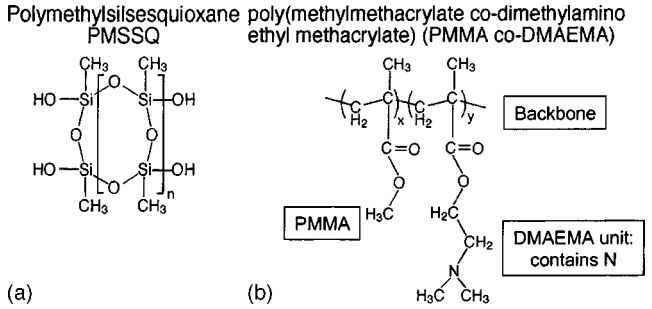

FIG. 1. Chemical structure of: (a) PMSSQ monomer and (b) porogen material PMMA-co-DMAEMA.

ment of materials and processes which lead to nanoporous low-*k* dielectrics, where the effective dielectric constant is a volume-weighted average of the *k* values of the dielectric matrix and the nanopores formed within it ($k=1$). Porous low-*k* films can be produced from mixing low-*k* matrix precursor material with sacrificial "porogen" material and then spincasting the mixture. The inorganic-based matrix material will react to form a crosslinked mechanically rigid structure, while the porogen material will evaporate to leave a network of nanopores, thereby reducing the effective *k* value of the nanoporous composite. Thermally decomposable organic material is used as the porogen, leading to nanoscale-sized pores.[2]

However, producing the desired nanopore structure in the low-*k* material is not simple. Significant manufacturability and reliability problems have been identified, such as porogen connectivity,[9] low stiffness of the porous structure,[10] and inhomogeneous of pore size,[11] and other mechanical problems with the integration process.[12] The nanoporous material—and processes to make it—must assure reasonably optimal porosity, pore size, and distribution, and homogeneous spatial distribution of the pores. In turn, this means that the precursor materials and their thermal transformations required for nanoporous low-*k* formation must be carefully designed, including matrix crosslinking, phase separation, and porogen decomposition, as well as precursor chemistry, and miscibility of matrix and porogen, all of which influence the final materials nanostructure achieved.[13]

II. RESEARCH APPROACH

This work, along with its predecessors, is aimed at understanding the thermal transformations of polymethylsilsesquioxane (PMSSQ)–porogen composite precursors as they lead to nanoporous low-*k* thin films. In this work, we investigate these transformations by observations of surface and thin-film properties as well as gas phase reaction products. Furthermore, we compare two different PMSSQ precursor formulations, which involve different concentrations of Si–OH groups in the PMSSQ precursor.

In our experiment, we chose the organosilicate material PMSSQ ($SiO_{1.5}CH_3$) for the low-*k* matrix. This material is a leading candidate for industry because of low-dielectric constant ($k=2.7-2.9$), high mechanical strength, good thermal stability, and low water uptake.[14] The chemical structure of

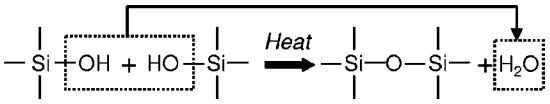

FIG. 2. PMSSQ matrix reaction, leading to crosslinking and H_2O release.

the PMSSQ precursor is shown in Fig. 1(a). By incorporating nonpolar, hydrophobic, and space occupying CH_3 (methyl) groups, the lower dielectric constant of the Si–O network is achieved. The monomers shown react at OH sites, causing polymerization and releasing H_2O as a byproduct of the crosslinking reaction, as shown in Fig. 2.

Polymethylmethacrylate-co-dimethylaminoethylmethacrylate (PMMA-co-DMAEMA) is used as the thermally decomposable organic material, thus serving the function of a porogen material. When 40% of PMMA-co-DMAEMA is added to PMSSQ matrix, the refractive index is 1.23 ~1.25, and the corresponding dielectric constant is 1.95.[6] The PMMA-co-DMAEMA, schematically shown in Fig. 1(b), is a random copolymer with monomer ratio 75/25. The tertiary amino group in the DMAEMA enhances the miscibility between matrix and porogen materials through hydrogen bonding to the hydroxyl group in the matrix.

The schematic process flow for thermal curing to produce the nanoporous PMSSQ-based low-*k* dielectric thin film is shown in Fig. 3. A solution of matrix precursor, porogen, and solvent is uniformly dispersed on the substrate by spincoating the wafer. Upon thermal cycling from room temperature to 450 °C, first the solvent evaporates, then PMSSQ crosslinking begins along with nanophase separation of matrix and porogen, and finally porogen species are volatized and thus evacuated from the material to form the low-*k* thin film. These transformations have been observed using a variety of techniques in the present work. Surface analysis methods, including time of flight-secondary ion mass spec-

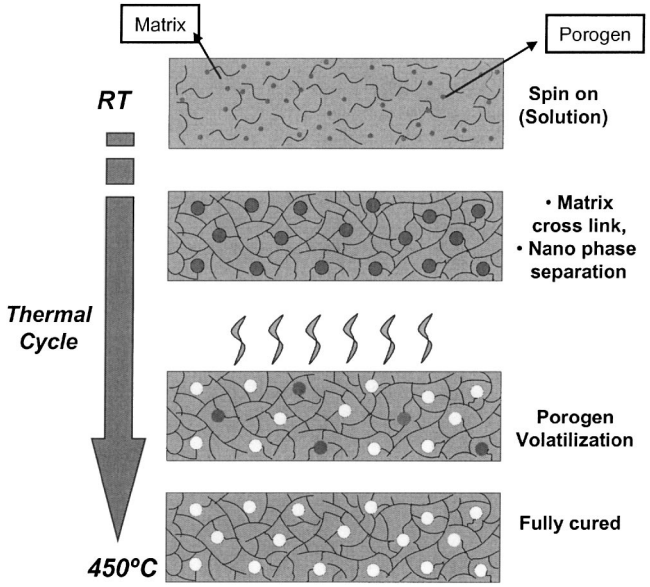

FIG. 3. Schematic behavior for forming nanoporous low-*k* through matrix crosslinking and porogen volatilization as consequence of thermal curing.

trometry (TOF-SIMS) and x-ray photoelectron spectroscopy (XPS), and thin-film analysis by small-angle neutron scattering (SANS) revealed the kinetics of matrix crosslinking, while thermal desorption mass spectrometry (TDMS) showed the evolution of gaseous reaction products from porogen and matrix during the complex chemical transformations which occur with thermal cycling from 100 °C to 450 °C.

III. EXPERIMENTAL DETAILS

Two different PMSSQ precursors were obtained from different suppliers in order to investigate the influence of initial precursor formulation on matrix crosslinking kinetics. These precursors were distinguished by differing concentrations of hydroxyl (OH) end groups [seen in Fig. 1(a)] relative to CH_3 groups in the same chemical bonding sites. We denote the two formulations we used as "low SiOH" and "high SiOH." While the details of these formulations are typically proprietary, we expected—and observed—that the kinetics of matrix crosslinking did in fact differ significantly for these two formulations, so that at least a qualitative trend can be inferred from the results.

Solutions of PMSSQ (8% by weight) and PMMA-co-DMAEMA (30% by weight) were dissolved in 1-methoxy-2-propanol solvent. The porogen used in the low–SiOH PMSSQ experiments was deuterated to distinguish PMMA and DMAEMA more clearly in neutron scattering experiments.

The films were prepared by spincoating the solution onto 1 in. silicon wafers at 3000 rpm for 30 s, attaining a film thickness of about 0.5 μm. After spinning, each film was cured in an inert gas furnace whose temperature was raised at 10 °C/min ramp rate to the selected temperature (in the range of 50–450 °C), cured at this temperature, and then cooled back to room temperature. Curing recipes were: 2–3 min at 50 °C, 120 min at 450 °C, and 60 min for temperatures between 50 and 450 °C.

TOF-SIMS studies were carried out at ITC-irst, Trento, Italy, using an ION-TOF TOF-SIMS IV instrument, which has a very high mass resolution [$\sim 5000@^{28}Si^+$ full width at half maximum (FWHM)/ $\sim 4000@^{16}O^-$ (FWHM)] that enables the differentiation of minute differences between masses. TOF-SIMS was performed in both static and dynamic modes. In static secondary ion mass spectrometry (SIMS) measurements, pulsed Ga^+ beam was used at 11 keV at low currents in order to assure that measurements did not see the consequences of surface damage by previous ion dose, and to minimize fragmentation. In the case of low-SiOH PMSSQ films, we observed that porogen species were depleted at the surface, so we used pseudo-dynamic-SIMS to observe a subsurface region approximately one-fifth of the film thickness below the surface by first removing surface material with a 10 keV Cs^+ beam as a sputtering beam and then using Ga^+ at 25 keV as the analysis beam. While the SIMS event inherently fragments and modifies the material in generating a group of secondary ions, we found that these fragmentation patterns show clear chemical trends and turn out to be extremely useful. Further details of the TOF-SIMS experiments and analysis have been given elsewhere.[7]

TDMS was performed at the University of Maryland to analyze volatile products of the curing process in the gas phase. A quadrupole mass spectrometer (INFICON, Transpector CIS 200) with an atomic mass range of 0–200 amu was directly installed into an ultrahigh vacuum (UHV) system for *in situ* real-time monitoring during vacuum curing. Emission current, electron energy, and electron multiplier values were 0.2 mA, 35 V, and 1 kV, respectively. For this analysis, samples were spun onto a 4 in. silicon wafer, then cured at 50 °C for 2 min to remove the solvent. The sample was then loaded on the resistive substrate heater inside the vacuum chamber and evacuated to 10^{-8} Torr. The resistive heater was prebaked to minimize outgassing from heater surface during TDMS experiments. Thermal desorption measurements were made by raising the substrate (heater) temperature 10 °C/min from room temperature to 450 °C.

SANS was used with a deuterated PMMA-co-DMAEMA porogen to understand the morphological development of the films during the curing process. These experiments were carried out at the Center for Neutron Research at the National Institute of Standards and Technology (NIST) using the 30 m NIST-NG7 instrument. Thin films were spincoated on 1 in. diameter silicon wafers and measured with the neutron beam incident along the surface normal. The SANS experiments were done with *in situ* curing up to 300 °C, and with higher curing temperatures to 450 °C done *ex situ* in a laboratory furnace. The wavelength, λ, was 8 Å with a wavelength spread, $\Delta\lambda/\lambda$, of 0.22. Sample to detector distances of 1.5 m and 11.75 m were used, which gave a q range of 0.0028–0.3 $Å^{-1}$. Four or more samples were stacked to increase the scattering volume. This technique has been used for the study of thin polymer films on silicon substrates by SANS.[15,16] After degradation of the deuterated PMMA-co-DMEAMA porogen to form pores, there is very little neutron scattering contrast between the PMSSQ matrix and the pores.

XPS was performed at ITC-irst using a Scienta ESCA-200 instrument with monochromatic source, using Al $K\alpha$ x rays (1486.6 eV) with a spectrometer energy resolution of 0.4 eV. No flood gun was used during measurement, since no charge compensation was needed. Emitted photoelectrons were collected at normal incidence, defining an information depth of about 8 to 10 nm.

IV. POLYMETHYLSILSESQUIOXANE MATRIX TRANSFORMATION

A. Crosslinking and dehydration

Figures 4(a) and 4(b) show on a linear scale the variation of TOF-SIMS secondary ion currents obtained from high–SiOH PMSSQ films by TOF-SIMS as a function of curing temperature, for negative [Fig. 4(a)] and positive [Fig. 4(b)] ions. These data are normalized to the intensities obtained from the sample cured at 50 °C. Although the presence of oxygen is known to influence the positive ion yield, it was

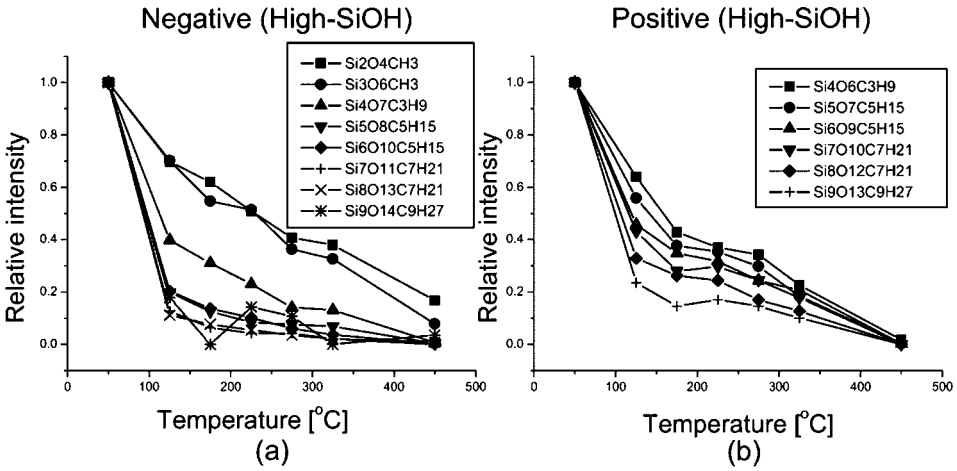

FIG. 4. TOF-SIMS yield of: (a) negative and (b) positive ions for high-SiOH PMSSQ with 30% porogen.

clearly observed that the intensities of positive and negative species are proportional over a significant number of ion species, such as those depicted in Fig. 4. This suggests that matrix effects in the TOF-SIMS measurement are small.[7,17] The negative ions are distinguished by having an extra oxygen atom in the fragment measured, associated with an extra electron on the additional oxygen atom, while the positive ions typically involve an ionized Si atom. These secondary ion fragments, produced by the incident ion bombardment, were reproducibly observed in the mass spectra and are utilized as key species involved in the thermal transformations of the material. They were identified by comparing the mass values of conjectured chemical structures composed of PMSSQ elements with the mass values of the key species. More detail of the fingerprint analysis is well described in our previous paper.[7]

These key species in the figures show characteristic patterns as a function of temperature, roughly similar in shape for all fragments. The intensity of all species decreases sharply for curing temperatures around 100 °C–200 °C, followed by slower decrease at higher temperatures. The relative rate of intensity decreases changes with the mass of the fragment, with larger mass species decreasing faster than small mass fragments.

Because the intensity of the key species (e.g., Fig. 4) would seem to be proportional to the amount of unreacted PMSSQ precursor, the intensity decrease upon curing temperature can be interpreted as a direct observation of crosslinking of the PMSSQ precursors with thermal curing. Accordingly, the results in Fig. 4 suggest that most crosslinking occurs around 100–200 °C, with the remainder continuing at a modest rate up to 450 °C. As shown in Fig. 2, the crosslinking occurs through reaction at the hydroxyl sites of the oligomer, generating an H_2O reaction product which should be volatile at curing temperatures in the range of 200 °C or above. *In situ* real-time TDMS results in Fig. 5 show that desorbing species at amu 18 are observed with increasing intensity in the range of 100–175 °C, indicative of H_2O desorption products from the high-SiOH film, which finally decreases at higher temperatures as the crosslinking reaction is completed. This temperature regime for dehydration corresponds to that observed by TOF-SIMS (Fig. 4) for matrix crosslinking temperatures. Both the TDMS and TOF-SIMS show persistence of the crosslinking and H_2O evolution to temperatures well above 200 °C; this is consistent with steric hindrance of the hydroxyl group by the presence of large methyl groups.[18]

B. Precursor formulations

The high-SiOH and low-SiOH formulations of PMSSQ precursors contained different concentrations of hydroxyl groups, cf. CH_3 groups, as explained above. As described elsewhere,[7] this compositional difference was directly in the relative intensity of twin peaks in the spectra for various secondary ion fragments, where the twin peaks arise from varying ratios of OH and CH_3 groups on the monomer, and the identification of the twin peaks was definitive from the known mass difference (1.98 amu) between the CH_3 (15.0235 amu) and OH (17.0027 amu) moieties. The relative intensity of the OH-related peaks was 1.5–2.0× higher in the high-SiOH material cf. the low-SiOH material.

The linear plots in Fig. 6 compare TOF-SIMS intensity variation of key species from the high-SiOH and low-SiOH PMSSQ as a function of temperature. To give a clear comparison of how the initial precursor formulation influences

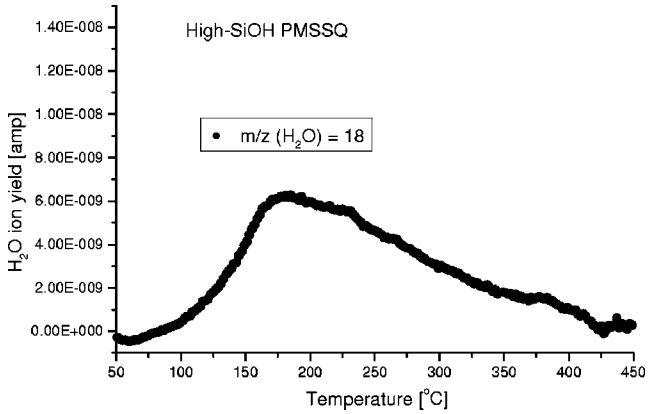

FIG. 5. Thermal desorption of H_2O reaction product from matrix crosslinking, detected by TDMS.

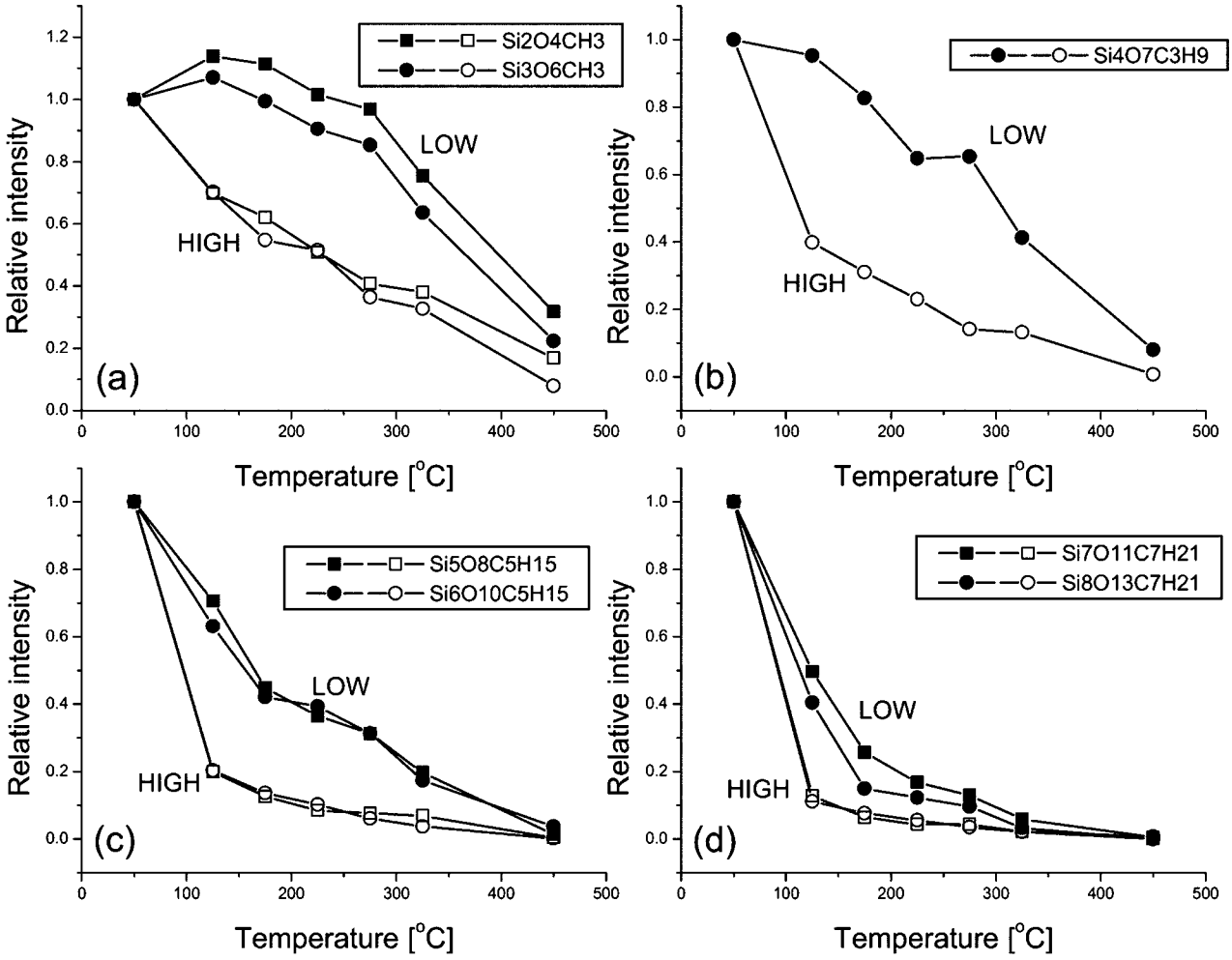

FIG. 6. TOF-SIMS (negative ion) comparison of matrix crosslinking kinetics for high-SiOH and low-SiOH PMSSQ precursor formulations.

the matrix transformation, seven key species are shown separately to present secondary ion fragment data from $Si_2O_4CH_3$ to $Si_8O_{13}C_7H_{21}$. The ion yields for the high-SiOH formulation drops considerably faster with curing than does the low-SiOH case, indicating a more rapid crosslinking reaction for the high-SiOH precursor formulation. For example, in Fig. 6(c) for Si5 and Si6 species at 175 °C, the high-SiOH intensity has dropped almost 90%, cf. only 60% for the low-SiOH case. Since secondary ion currents are taken as indicative of the crosslinking of the matrix, these results imply that crosslinking is faster for high-SiOH content formulations of PMSSQ than for low-SiOH versions. This might be expected in part because of the high density and closer average proximity of OH moieties, both of which would tend to enhance crosslinking and H_2O release.

V. PHASE SEPARATION

SANS was used to study the film's behavior during curing. SANS data for low-SiOH PMSSQ/30% porogen films after curing at different temperatures are shown in Fig. 7. Deuterated porogen was employed to enhance neutron scattering contrast for the system. The scattered intensity varies as a function of curing temperature due to morphological changes occurring in the samples. The scattering intensity changes markedly from the as-spun material (25 °C) to that seen at 125 °C, with the increased SANS intensity at 125 °C indicates the phase separation of the porogen from the PMSSQ matrix, forming a porogen domain structure distributed in the matrix. The scattering is nearly unchanged as the temperature is then increased up to 300 °C, which indicates that the morphology is essentially unchanged over this temperature range. The initial as-spun morphology is undoubtedly in a metastable state due to the rapid evaporation of the solvent. Upon curing it begins to coarsen, eventually becoming frozen by the crosslinking of the matrix. At the highest temperature (450 °C) the scattering drops dramatically due to a loss of contrast as the deuterated porogen is volatilized to form the nanopores in the films.

During curing, the MSSQ precursors lose -OH groups because of crosslinking, which makes the system lose miscibility and phase separate. The broad SANS peak indicates a broad distribution of pore size and distribution. One can expect to get smaller pore sizes by using high-SiOH PMSSQ, because the improved miscibility will prevent phase separation. Therefore, a major challenge is to design materials and

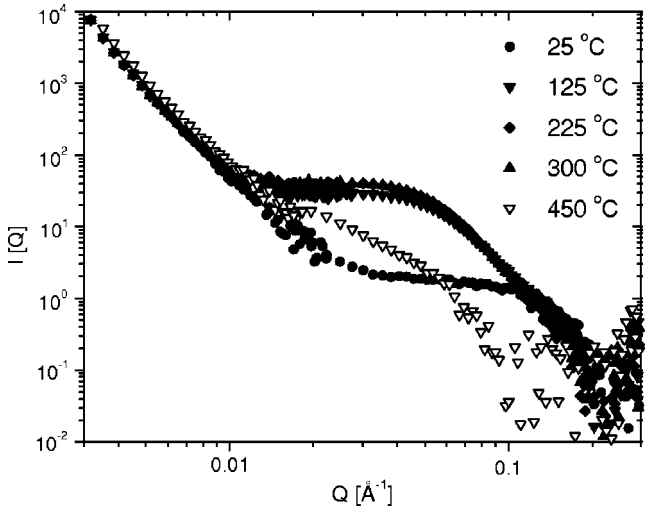

FIG. 7. SANS data for low-SiOH PMSSQ with 30% porogen cured at different temperatures.

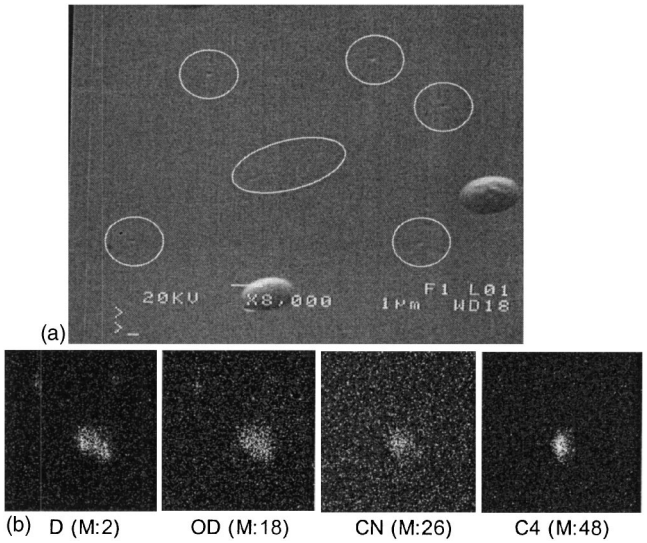

FIG. 8. (a) SEM micrograph showing the voids (encircled) and two porogen particles on low-SiOH PMSSQ cured at 275 °C. (b) High magnification TOF-SIMS images for porogen markers from low-SiOH PMSSQ cured at 275 °C.

processes which assure nanophase separation that leads to an ideal nanoporous structure of the PMSSQ matrix.

VI. POROGEN AGGLOMERATION

The kinetics of matrix crosslinking might also affect porogen phase separation. The higher crosslinking reaction rate in high-SiOH PMSSQ precursor will tend to freeze the dielectric matrix, trap the porogen species, and prevent porogen diffusion and agglomeration, thus preserving a nanophase distribution of porogen moieties. As a consequence, optimized precursor formulations play an important role in determining the final nanostructure of these nanoporous low-*k* dielectric materials.

The agglomeration of porogen in the low-SiOH case is additional evidence for the importance of crosslinking kinetics compared to porogen diffusion kinetics. The scanning electron microscopy (SEM) image in Fig. 8(a), for low-SiOH PMSSQ sample with 30% porogen after curing at *T* higher than 275 °C, shows the occurrence of at least two phenomena, namely void formation and particle formation. Voids are highlighted within the circles in this figure. The particles are larger ($\sim$1 μm in diameter) and can be easily recognized, e.g., in optical microscopy. Particle density (i.e., number per unit area) increases with curing in the temperature range of 225–325 °C. TOF-SIMS shows that the particles are composed of porogen species. The lateral distribution maps of DMAEMA, PMMA, and porogen backbone markers [shown in Fig. 8(b)], in fact, match particle positions. Because of the presence of backbone species in the particles, we conclude that they are not formed by ligand reagglomeration. Upon increasing the curing temperature, ratios of DMAEMA to PMMA characteristic species (specifically, CN/D) decrease in the particles because the porogen species undergo preferential loss of DMAEMA ligands. The particles thus become PMMA enriched until they completely disappear because of thermal degradation of the residual PMMA and porogen backbone.

In addition, high magnification TOF-SIMS imaging (10 $\times$10 μm^2) shown in Fig. 8(b) point out that the lateral distribution of PMMA species—D (M:2) and OD (M:18)—is more scattered than other species like CN (M:26) and C4 (M:48). Based on that, we conclude that the segregation of porogen species during phase separation is more complex. Indeed, the segregation of some porogen markers is observed in other positions than the particles, namely where the voids are present. This suggests that aggregation of partially PMMA-enriched porogen can also take place.

No porogen agglomerates were observed for the high-SiOH samples, confirming that the higher SiOH content causes a faster phase separation and freezing of the nanostructure due to the more rapid matrix crosslinking. Investigations of the relationship between initial precursor functionality and resulting pore size distribution have been previously reported.[6,13] A higher level of miscibility for high-SiOH PMSSQ slows phase separation between matrix and porogen material and finally leads to smaller porogen domains. The more rapid crosslinking of the matrix acts to reduce porogen diffusion rates and trap the porogen nanoclusters. In contrast, the lower miscibility of low-SiOH PMSSQ and its slower matrix crosslinking may yield larger porogen domains associated with more facile porogen diffusion in low-SiOH PMSSQ film.

VII. THERMAL DECOMPOSITION OF POROGEN MATERIALS

Porogen decomposition process was analyzed by TDMS, TOF-SIMS, and XPS. As porogen material is thermally decomposed upon curing, volatile fragments are released from the film to leave open nanopores, thereby reducing the effective dielectric constant of the film substantially. This is revealed in the observation of gas phase products and changes in the surface composition of the film.

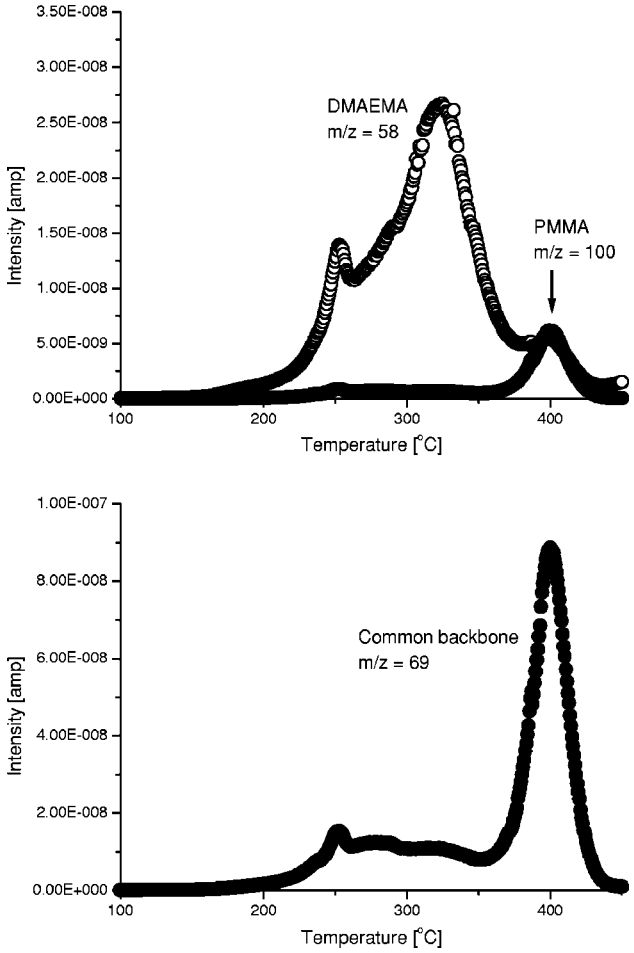

FIG. 9. Thermal desorption of porogen fragments from high-SiOH PMSSQ material with 30% porogen: (a) DMAEMA ligand and PMMA ligand; and (b) Common backbone.

A. Thermal desorption mass spectroscopy

The TDMS result for $m/z=58$ amu, a DMAEMA decomposition product containing tertiary amino group, is shown in Fig. 9(a) as a function of temperature. Generation of this DMAEMA-related product is strongest in the range of 200–350 °C, though some additional decomposition occurs at an even higher temperature. The remaining DMAEMA backbone gives rise to desorption of a product released as $m/z=69$ amu. As seen in Fig. 9(b), this DMAEMA backbone product is primarily volatilized at 400 °C, i.e., a substantially higher temperature than seen for most of the tertiary amine product of DMAEMA. This comparison demonstrates that most of the DMAEMA component is thermally fractured upon curing, splitting off the ligand including the tertiary amino group from the parent DMAEMA monomer.[19] It should be noted that a small component of the $m/z=69$ spectrum reflects TDMS structure similar to that of the tertiary amine, and vice versa, indicating some interaction between these two components of DMAEMA.

Small amount of desorption of PMMA-related species is observed at $m/z=100$ amu, as shown in Fig. 9(a). This is attributed to the parent ion of the PMMA monomer. PMMA degradation is reported in the literature to entail the generation of monomer MMA products which are unzipped from PMMA chains.[20] This desorption trend suggests that the PMMA molecules are decomposed in the temperature range of 350–450 °C, which in turn corresponds to thermogravimetric analysis results in the literature.[21,22] While not readily observed in Fig. 9(a), we did measure a small amount of $m/z=100$ amu release in the lower-temperature region corresponding to the DMAEMA tertiary amine product, indicating some coupling and interaction of the two components in the copolymer porogen.

B. Time-of-flight secondary ion mass spectroscopy

The corresponding changes in porogen content with curing as seen at the surface by TOF-SIMS are given in Fig. 10, which shows data for fragments characteristic of the DMAEMA components, the PMMA components of the monomeric units and porogen backbone species. For the high-SiOH material in Fig. 10(a), the data are readily obtained using conventional static SIMS (i.e., TOF-SIMS), since appreciable porogen is present at the surface. For the low-SiOH material in Fig. 10(b), however, porogen is depleted at the surface,[7] as mentioned above. Therefore, observation of porogen concentration required the use of pseudo-dynamic SIMS, such that the surface layers were removed by Cs^+ sputtering and then examined by conventional TOF-SIMS.

Although a considerably larger number of porogen-related fragments were observed in our studies, we chose here to emphasize uniquely identifiable markers for the separate components in the porogen. CN is undoubtedly related to DMAEMA because of the amine group, which is present in the identifying DMAEMA ligand but not in that of the PMMA ligand. Similarly, CH_3O can be related to the PMMA ligand because no other part of the PMMA or DMAEMA molecule is apt to produce this fragment. Other fragments we observed included representatives (e.g., C_4H_5O, C_5) of the porogen backbone common to both DMAEMA and PMMA.

As seen in Fig. 10 for both high- and low-SiOH samples, the DMAEMA content (seen as CN) is depleted significantly in the temperature range of 225–325 °C, while species reflective of the common porogen backbone (C_4H_5O) were relatively unaffected by curing in this temperature regime. While a slight increase in yield is seen in the temperature region (100–300 °C) in both figures, we consider this simply noise. In contrast, the intensity of the PMMA ligand (seen as CH_3O) begins a substantial decrease only at a considerably higher temperature, around 325 °C. The common backbone of the porogen follows a temperature dependence similar to that of the PMMA ligand. This behavior of the PMMA monomer is in reasonably good agreement with prior thermogravimetric analysis results.[20,21]

While the pseudo-dynamic SIMS mode raises questions for molecular analysis associated with sputter damage, the porogen species were analyzed by comparisons involving numerous fragments and by concentrating on trends with thermal curing. In addition, deuterated PMMA was employed in the low-SiOH PMSSQ samples, so that it could be used to clearly identify the PMMA components of the poro-

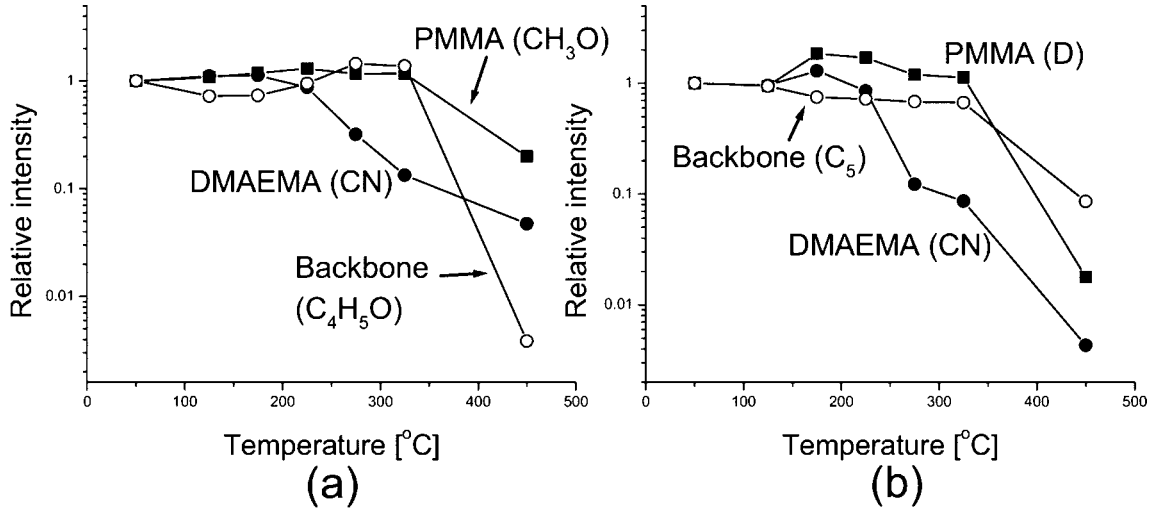

FIG. 10. TOF-SIMS porogen analysis comparing DMAEMA and PMMA fragment concentrations as seen for: (a) high-SiOH material using static TOF-SIMS (negative ion) and (b) low-SiOH using pseudo-dynamic TOF-SIMS (negative ion).

gen. Nitrogen-containing species were assigned as DMAEMA species, and the large carbon cluster C_5 was considered as indicative of the porogen backbone.

With these considerations, the TOF-SIMS results clearly show a similar behavior for porogen release from high-SiOH and low-SiOH material, in which the nitrogen-containing DMAEMA ligand is desorbed in the range of 225–325 °C, and the PMMA and porogen backbone species are released above 325 °C. This picture is in good agreement with the conclusions from thermal desorption mass spectroscopy described above.

C. X-ray photoelectron spectroscopy

XPS was also performed to analyze the surface characteristics of low- and high—SiOH PMSSQ. The C(1*s*) core-level spectra are shown in Fig. 11 for as-deposited material without porogen, as well as the dependence of these spectra on curing for 30% porogen content. For the as-deposited material, a low-temperature bake at 50 °C was carried out for low-SiOH and high-SiOH samples for 2 and 3 min, respectively, to assure complete solvent evaporation.

The XPS spectra show differences: (1) Between the high-SiOH and low-SiOH samples for pure PMSSQ, and (2) as a function of curing in 30% porogen samples. The analysis of the spectra is aided by our knowledge of the XPS instrument's resolution and line shape, as well as by line shape analysis algorithms we have developed and used extensively. There are at least three to four peaks in the spectra, a main peak (Region C1–C2), a smaller peak C5, a shoulder (Region C3–C4), and perhaps a peak in Region C6. The approximate binding energies for various C moieties are known: C–H, and C–C bonds in the C1–C2 region, C–O and C═O bonds in the C3–C4 region, O═C–O bonds in the C5 region, and C–Si bonds in the C6 region. Since C–H and C–C bonds are usually 0.7–0.8 eV apart, and additionally C–O and C═O bonds are also separated in energy,[23] we identify C1 and C2 as separate peaks, and the same for C3 and C4. The energy resolution of the XPS instrument is sufficient to resolve these structures, and improved line shape fitting is achieved in this way. C–H (Peak C1) and C–C (Peak C2) moieties are present in both high-SiOH and low-SiOH samples. In addition, a C═O component (Peak C4) is needed to fit the high-SiOH spectrum, so that C4 is regarded as characteristic of high-SiOH PMSSQ.

Components C3 and C5 were required to account for the full spectra of the porogen-containing samples. The chemical shift of Peak C3 from the binding energy of saturated hydrocarbon Peak C1 (285.0 eV) is around 1.6 eV, while peak C5 is shifted to 289.4 eV. Therefore, we assign Peak C3 to C–O bonds and Peak C5 to O═C–O configuration in the PMMA chemical structure. Both peaks disappear when curing temperature reaches to 450 °C, which supports their assignment as porogen-related components. No differences were observed by varying emission angle, indicating that the spectra are representative of the thin-film material, undistorted by an appreciable adsorbed species.

The XPS spectrum for the nitrogen 1*s* core level was also detectable at a binding energy range typical for C–N or O–C–N bonds. The N(1*s*) core line disappeared above about 225 °C, consistent with its origin in the DMAEMA N-containing ligand which was shown above to be released from the material at this temperature. The low intensity of N in the spectra prevented any identification of chemical shifts associated with N-bonding configurations.

Once 450 °C curing has taken place, the high-SiOH and low-SiOH C(1*s*) spectra in Fig. 11 are identical. The differences between high-SiOH and low-SiOH spectra at lower curing temperature signifies the different reaction kinetics of the materials, while the similarity of spectra for 450 °C curing results from the completion of matrix crosslinking and porogen volatilization, leading to low-*k* matrix material with the same chemical structure. These XPS observations are consistent with the results and conclusions from the TOF-SIMS and TDMS experiments.

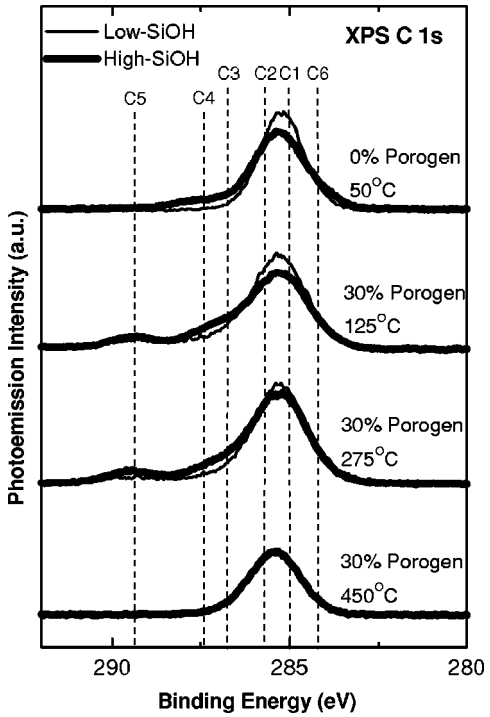

FIG. 11. XPS results comparing low-SiOH and high-SiOH PMSSQ material for: As-deposited 0% porogen (Sample 1); 30% porogen cured at 125 °C (Sample 2); 30% porogen cured at 275 °C (Sample 6); and 30% porogen cured at 450 °C (Sample 8).

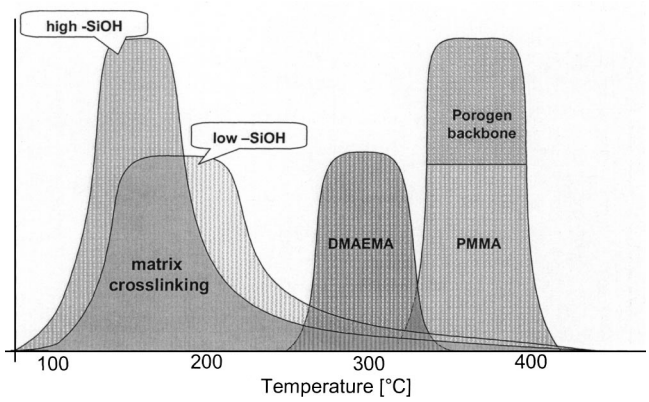

FIG. 12. Schematic depiction of overall chemical transformation kinetics to form nanoporous PMSSQ low-*k* dielectric material, as derived from this work.

VIII. DISCUSSION

These results convey a picture of the thermal transformations which occur in the porogen-mediated formation PMSSQ-based nanoporous low-*k* dielectric films. A schematic representation of the temperature-dependent behavior in these systems is presented in Fig. 12. As needed to stabilize a nanopore structure within the matrix material, the crosslinking of the matrix occurs at lower temperatures in the range of 100–200 °C, during which the porogen serves as a space-filling agent. The kinetics of matrix crosslinking is more rapid for higher concentrations of SiOH moieties in the PMSSQ precursor. At higher temperatures, the porogen begins to decompose, first through evolution of N-containing DMAEMA-specific ligands in the range of 200–350 °C, while the remainder of the DMAEMA and also the entire PMMA components remain. Finally, remaining porogen species are volatilized at the highest temperatures, above 300 °C. While generally separated by temperature ranges, there is some interaction between the decomposition of the DMAEMA ligand and the other porogen components.

While this picture provides substantial insight into the relative kinetics of thermal transformations in these materials, it is admittedly an incomplete picture. One can envision much more detailed kinetics arising from more complex thermal cycling, e.g., varying temperature ramp rates or even programmed ramp-and-hold recipes. Even in these cases, the extraction of truly fundamental kinetic behavior remains a challenge, as witnessed even in the complexity of interpretation for thermal desorption spectroscopy from well-defined adsorbates on surfaces. Therefore, we believe the simpler thermal cycles investigated here have returned substantial insight for the effort, and added distinctly to chemical and materials insights.

It is gratifying to find that the surface and gas phase analytical methods give a consistent picture of the evolution of the nanoporous low-*k* material. To first order, what leaves the surface of the material is seen in the gas phase as a reaction product, either the H_2O product from crosslinking of the PMSSQ matrix, or at various higher temperatures the volatile products from porogen decomposition and desorption. Of course, understanding the kinetics in detail presents a complex and more serious challenge for both surface and gas phase analysis. For the surface spectra, surface concentrations are influenced by any segregation phenomena which are present (e.g., surface depletion of porogen in the case of low-SiOH), and by the time-history of the thermal cycle (where in principle temperature-dependent surface segregation could occur, or where there could be hysteresis or time-lag effects that depend on temperature ramp rates). The latter phenomena could influence the thin-film measurements by SANS as well. The quantitative dynamics seen by thermal desorption mass spectrometry is influenced by similar effects as well as by the residence time of desorbing species in the TDMS chamber. Despite the complexity of such details, a consistent picture emerges of the relative kinetics for matrix crosslinking and porogen evolution, which together determine the nanoscale structure of the nanoporous low-*k* material.

The difference in matrix crosslinking kinetics for high-SiOH versus low-SiOH films is significant to the resulting nanostructure. As seen clearly in the TOF-SIMS measurements, the high-SiOH precursor formulation undergoes reactive cross-linking faster than does the low-SiOH material, providing a higher margin of safety against porogen diffusion, which would likely lead to porogen agglomeration and pore sizes too large for material requirements of the technology: If pore sizes are too large, pore connectivity is more likely, and distributions of micro-properties (e.g., local dielectric constant) may be nonuniform. Indeed, the porogen

agglomerates observed in TOF-SIMS images for low-SiOH are testimony to this effect. Basically, faster crosslinking is generally desirable to freeze out the possibility of porogen diffusion, in order to maintain small pores sizes.

The detailed TOF-SIMS spectra represent clear evidence of matrix crosslinking, although not in a directly quantitative manner. As the SIMS event generates fragmentation patterns which are sensitive to the residual amount of PMSSQ oligomers, the secondary ion intensity associated with these ions decreases as crosslinking and polymerization of the low-*k* precursors proceeds. It is clear that the TOF-SIMS measurements provide a valuable monitor of the polymeric crosslinking reaction even if further theoretical treatments would be required to explain the detailed physics which causes the pattern to change. For instance, the larger the ions, the faster the intensity decreases. In general, it is difficult to quantify polymerization and crosslinking kinetics at the level of chemical bonds observed here. However, these results suggest that the very fragmentation so problematic in many mass spectroscopy applications may have unique advantages in the study of complex macromolecular materials systems. In such cases, for polymers or biomolecules, identifying medium-range chemical or molecular order is critical to understanding these macromolecular systems. Most chemical analyses sense either short-range molecular bonding (e.g., Raman, Fourier transform infrared) or average long-range properties (e.g., molecular weight). Here, the fragmentation associated with ion-induced decomposition displays fragmentation patterns indicative of medium-range molecular order.

IX. CONCLUSION

These results give insight into the thermal transformation kinetics of spin-cast porogen-containing low-*k* dielectric films as they evolve into nanoporous low-*k* materials suitable for advanced semiconductor interconnect technology. PMSSQ low-*k* material undergoes crosslinking reactions in the range of 100–225 °C, inhibiting diffusion of porogen-related species from PMMA-co-DMAEMA porogen. Porogen decomposition begins near 200 °C and is ligand selective, in that for the most part the N-containing ligand of DMAEMA is volatilized at considerably lower temperatures (~200 °C) than that (~400 °C) for the remaining species (the PMMA ligand and the common backbone for both PMMA and DMAEMA). Different formulations of the PMSSQ precursor alter the matrix crosslinking kinetics: Higher concentrations of Si–OH groups in the precursor, as compared to $Si-CH_3$ groups in their place, cause more rapid crosslinking reactions, presumably due to the higher concentration of reactants available for the crosslinking OH–OH bonds to form a bridging oxygen and release H_2O. The faster crosslinking in turn changes the ability for porogen species to diffuse; evidence for this may be contained in the observed depletion of surface porogen and the formation of porogen agglomerates, seen for the low-SiOH material but not for the high-SiOH material.

Finally, we believe this research demonstrates the inherent value of the analytical methods. By revealing a more detailed kinetic picture of the material transformations involved in forming nanoporous low-*k* thin films, it provides a firm experimental basis for evaluating materials designs, e.g., in seeking precursor formulations which crosslink the matrix rapidly to minimize porogen diffusion. In addition, the results illustrate the power of combining surface, thin-film, and gas phase analytical methods in achieving a self-consistent picture of the reaction phenomena.

ACKNOWLEDGMENT

This work has been partially supported by the Autonomous Province of Trentino Italy, the University of Maryland, IBM Research, and the National Institute of Standards and Technology.

[1] *The International Technology Roadmap for Semiconductors* (Semiconductor Industry Association, San Jose, California, 1997).
[2] K. Maex, M. R. Baklanov, D. Shamiryan, F. Iacopi, S. H. Brongersma, and Z. S. Yanovitskaya, J. Appl. Phys. **93**, 8793 (2003).
[3] M. Morgen, E. T. Ryan, J. H. Zhao, C. Hu, T. H. Cho, and P. S. Ho, Annu. Rev. Mater. Sci. **30**, 645 (2000).
[4] H. J. Lee, E. K. Lin, B. J. Bauer, W. L. Wu, B. K. Hwang, and W. D. Gray, Appl. Phys. Lett. **82**, 1084 (2003).
[5] T. Batchelder, W. Cai, J. Bremmer, and D. Gray, Solid State Technol. **42**, 29 (1999).
[6] Q. R. Huang, W. Volksen, E. Huang, M. Toney, C. W. Frank, and R. D. Miller, Chem. Mater. **14**, 3676 (2002).
[7] P. Lazzeri, G. W. Rubloff, L. Vanzetti, R. M. Briber, M. Anderle, M. Bersani, J. J. Park, H. C. Kim, W. Volksen, R. D. Miller, and Z. Lin, Surf. Interface Anal. **36**, 304 (2004).
[8] N. Aoi, Jpn. J. Appl. Phys., Part 1 **36**, 1355 (1997).
[9] M. P. Petkov, M. H. Weber, K. G. Lynn, and K. P. Rodbell, Appl. Phys. Lett. **79**, 3884 (2001).
[10] J. Gross, J. Fricke, R. W. Pekala, and L. W. Hrubesh, Phys. Rev. B **45**, 12774 (1992).
[11] H. J. Lee, C. L. Soles, D. W. Liu, B. J. Bauer, E. K. Lin, W. L. Wu, and A. Grill, J. Appl. Phys. **95**, 2355 (2004).
[12] L. L. Mercado, S. M. Kuo, C. Goldberg, and D. Frear, IEEE Trans. Adv. Packag. **26**, 433 (2003).
[13] Q. R. Huang, H. C. Kim, E. Huang, D. Mecerreyes, J. L. Hedrick, W. Volksen, C. W. Frank, and R. D. Miller, Macromolecules **36**, 7661 (2003).
[14] P. S. Ho, J. Leu, and W. W. Lee, *Low Dielectric Constant Materials for IC Applications*, Advanced Electronics vol. 9 (Springer, Berlin, 2003), pp. 173–175.
[15] D. L. Ho, R. M. Briber, R. L. Jones, S. K. Kumar, and T. P. Russell, Macromolecules **31**, 9247 (1998).
[16] R. L. Jones, S. K. Kumar, D. L. Ho, R. M. Briber, and T. P. Russell, Macromolecules **34**, 559 (2001).
[17] P. Lazzeri, L. Vanzetti, E. Iacob, M. Bersani, M. Anderle, J. J. Park, Z. Lin, R. M. Briber, G. W. Rubloff, and R. D. Miller, *Proceedings of the 2003 International Conference on Characterization and Metrology for ULSI Technology*, Austin, TX, 24-28 March 2003.
[18] W. E. Wallace, C. M. Guttman, and J. M. Antonucci, Polymer **41**, 2219 (2000).
[19] S. B. Tan, L. M. Zhang, and Z. M. Li, J. Appl. Polym. Sci. **69**, 879 (1998).
[20] G. Montaudo, C. Puglisi, and F. Samperi, J. Polym. Sci., Part A: Polym. Chem. **36**, 1873 (1998).
[21] Z. Czegeny, E. Jakab, and M. Blazso, Macromol. Mater. Eng. **287**, 277 (2002).
[22] J. D. Peterson, S. Vyazovkin, and C. A. Wight, J. Phys. Chem. B **103**, 8087 (1999).
[23] G. Beamson and D. Briggs, *High-Resolution XPS of Organic Polymers-The SCIENTA ESCA300 Database* (Wiley, New York, 1992).